IL NUOVO CIMENTO **47 C** (2024) 257
DOI 10.1393/ncc/i2024-24257-x

COMMUNICATIONS: SIF Congress 2023

Charge-to-spin interconversion at (111) oxide interfaces

M. TRAMA([1])([2])([3])

([1]) *Dipartimento di Fisica "E. R. Caianiello", Universitá di Salerno - Fisciano, Italy*
([2]) *INFN Gruppo Collegato di Salerno - Fisciano, Italy*
([3]) *Institute for Theoretical Solid State Physics, IFW Dresden - Dresden, Germany*

received 6 February 2024

Summary. — In the field of spin-orbitronics, the intrinsic spin-orbit coupling (SOC) of materials is exploited to convert spin to charge and viceversa. The Edelstein effect is a peculiar spin-orbitronic phenomenon, typical of two-dimensional (2D) systems with SOC and broken inversion symmetry, where a magnetization is produced in response to an electric field. A natural platform to exhibit this feature are two-dimensional electron gases at oxide interfaces. Here we predict an Edelstein response at (111) $LaAlO_3/SrTiO_3$ interface, discussing in detail the differences with the canonical Edelstein effect in a simple isotropic Rashba model. We predict a tunable spin and orbital magnetization, commenting on the possibility of disentangling the two in order to exploit them theoretically and practically.

1. – Introduction

The field of Spintronics was born after the discovery of the Giant Magnetoresistance (GMR) [1], namely the increase in the resistance of a sample after the application of a magnetic field to the system. This is the basis for practical applications, such as Magnetic Random Memory Access (MRAM), which are in some cases faster and less energetically expensive than electronic devices. In spintronics [2] one can either generate a spin current after the application of electric fields, or, viceversa, generate current by manipulating the spin state of the system, *e.g.*, using magnetic fields. The usual way in which one can inject spin-polarized currents is through ferromagnetic metals which are connected to the device of interest. A limitation of this kind of approach is scalability: for the production of complex devices, one needs to manipulate a large number of ferromagnets [3].

A new path in the generation of the spin-polarized current is the use of intrinsic mechanisms in systems with strong spin-orbit coupling (SOC) [4]. Spin-orbitronics is a specific branch of spintronics for systems which possess a strong SOC. An applied electric field change the orbital motion of the electrons, which through SOC can translate into the establishment of a defined spin state. A prominent example is the Edelstein Effect

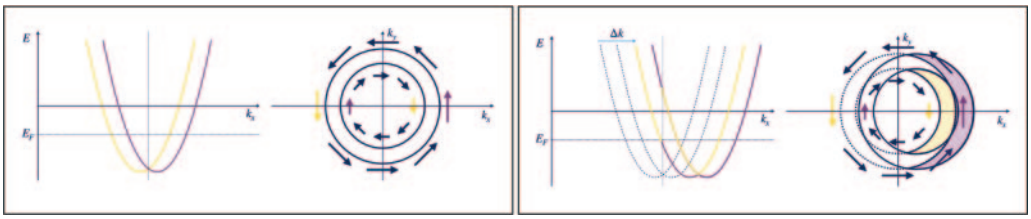

Fig. 1. – (Left panel) Energy spectrum sketch of Hamiltonian (1) along k_x and a benchmark Fermi surface with the projected spin state. The yellow and the purple color correspond to a pure S_y spin state. (Right panel) An electric field along the x direction breaks the equilibrium, shifting the band of Δk_x. The colored area highlight the spin accumulation for each single band shifted from the equilibrium. The sum of the two is non-zero due to the different areas.

(EE) [5], namely the generation of a (111) LAOmagnetization in response to an external electric field [6]. The key feature for realizing such an effect is the lack of inversion symmetry in two-dimensional (2D) systems with SOC. The combined effect of SOC and inversion symmetry breaking leads to the so-called Rashba SOC. Oxide heterostructures are the ideal platform to exhibit EE. Consider the prototype of the oxide interfaces, the $LaAlO_3/SrTiO_3$ (LAO/STO) interface [7]: a 2D electronic gas (2DEG) is formed at the interface due to a confining potential which is formed after the LAO is grown on STO [8-10]. The conduction band of the 2DEG is formed by the d-orbitals of the Ti atoms, thus inducing a strong SOC on mobile electrons. Moroever, since the Bloch wave functions possess an orbital angular momentum, also an orbital magnetization occurs, giving rise to the orbital Edelstein Effect (OEE) [4]. While the (001) interfaces has largely been investigated, the (111) trigonal interfaces have only now attracted attention due to their lattice geometry, similar to graphene [11] and thus able to manifest many non-trivial phenomena [12-14]. The EE and OEE at (111) LAO/STO interface have been considered only very recently [15]. In this paper, we provide a summary of the evidence on tunable EE and a OEE larger by an order of magnitude than the spin EE. The paper is organized as follows: in sect. **2** we provide the simplest isotropic Rashba model exhibiting EE; in sect. **3** we explain the low-energy region of a (111) LAO/STO interface with a tight-binding model and compute the EE in the semiclassical Boltzmann framework. In sect. **4** we discuss the results and give some future perspectives.

2. – Rashba-Edelstein effect in a simple Rashba Model

The phenomenology of EE consists in the generation of an in-plane magnetization $\vec{m}$ in response to an in-plane electric field $\vec{E}$ on the system, via the constitutive relation $m_\alpha = \chi_{\alpha\beta} E_\beta$, where $\chi_{\alpha\beta}$ is called Edelstein susceptibility. Since this susceptibility connects an axial vector (magnetization) with a polar vector (electric field), it is clear that inversion symmetry must be broken for the effect to show up. On the other hand, since the magnetization changes sign under time reversal, while the electric field does not, from Onsager's principle it follows that the tensor $\chi_{\alpha\beta}$ must be antisymmetric.

Let us consider the 2D Hamiltonian of a parabolic band with Rashba SOC

$$H = \beta k^2 - \alpha \left(\vec{k} \times \vec{\sigma} \right) \cdot \hat{z}, \tag{1}$$

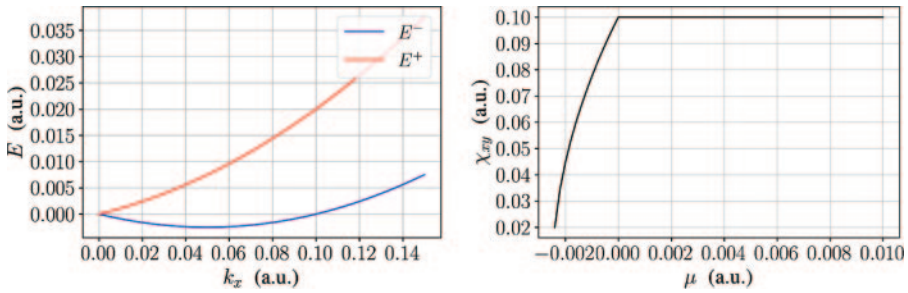

Fig. 2. – (Left panel) Detail of the band structure for benchmark parameters of $\beta = 1$ and $\alpha = 0.1$. E^+ and E^- refer to the two different eigenvalues of the Hamiltonian 1. (Right panel) Edelstein susceptibility for the same choice of parameters.

where $\vec{k}$ is the quasi-momentum of the electrons, $k^2 = k_x^2 + k_y^2$, $\vec{\sigma}$ is the vector of the Pauli matrices, and $\hat{z}$ is the unitary vector in the z direction. The Rahsba term generates the so-called spin-momentum locking, *i.e.*, at each $\vec{k}$ point in the Brillouin zone there is a definite spin direction of the Bloch functions. The eigenvalues and the spin projection on them are sketched in left panel of fig. 1. Consider now an electric field E along the x axis perturbing the system. Heuristically, this means that a shift in the quasi-momentum of the order of $\Delta k_x \approx -\frac{eE}{\hbar\tau_0}$ occurs, where τ_0 is the scattering time. In right panel of fig. 1 the effect on the Fermi surface is shown: the shift of the Fermi surfaces induces an imbalance of the spin along the y direction due to the spin-momentum locking. In order to quantify this picture we can consider the Boltzmann equation for an homogeneous medium and for stationary processes, $\frac{\mathrm{d}\vec{p}}{\mathrm{d}t} \cdot \vec{\nabla}_{\vec{p}} f = \text{Coll.}$, where $\vec{p} = \hbar\vec{k}$, f is the distribution function of the electrons and Coll. is the collisional terms of the electrons due to the scattering process. By approximating $\text{Coll.} = \frac{f_{\text{th}} - f}{\tau_0}$, where f_{th} is the thermal Fermi distribution, and $\frac{\mathrm{d}\vec{p}}{\mathrm{d}t} = e\vec{E}$, we can obtain the modification of the distribution function $\varphi = f - f_{\text{th}}$ due to the electric field as $\varphi = -\tau_0 e\vec{E} \cdot \vec{\nabla}_{\vec{p}} f_{\text{th}}$. The magnetization in the α direction is therefore proportional to integral over the Brillouin zone (BZ) of the spin value along α times the distribution function. The integral over the thermal distribution is zero due to the symmetry, therefore the only non-vanishing component is

$$m_\alpha = \frac{\mu_B S_{\text{cell}}}{\hbar} \int_{BZ} \frac{\mathrm{d}^2\vec{k}}{4\pi^2} \frac{\hbar}{2} \langle\sigma_\alpha\rangle\varphi(\vec{k}) = -\frac{e\mu_B\tau_0 S_{\text{cell}}}{2\hbar} \int_{BZ} \frac{\mathrm{d}^2\vec{k}}{4\pi^2} \langle\sigma_\alpha\rangle \frac{\partial f_{\text{th}}}{\partial k_\beta} E_\beta, \tag{2}$$

where μ_B is the Bohr magneton and S_{cell} is the area of the unit cell, and therefore $\chi_{\alpha\beta} = -\frac{e\mu_B\tau_0 S_{\text{cell}}}{2\hbar} \int_{BZ} \frac{\mathrm{d}^2\vec{k}}{4\pi^2} \langle\sigma_\alpha\rangle \frac{\partial f_{\text{th}}}{\partial k_\beta}$. The behaviour of χ_{xy} as a function of the Fermi energy μ for this simple model is depicted in fig. 2. The susceptibility for such a model saturates when the Fermi level crosses both bands.

3. – Spin and orbital Edelstein effect at (111) $LaAlO_3/SrTiO_3$ interface

Oxide interfaces are the natural candidate to possess interesting properties of spin-to-charge conversion.

Here we focus on the (111) LAO/STO interface. The 2DEG that is formed at the interface is confined in the first layers of the STO, therefore we take into account a minimal tight-binding bilayer model of Ti atoms of STO in the (111) direction whose

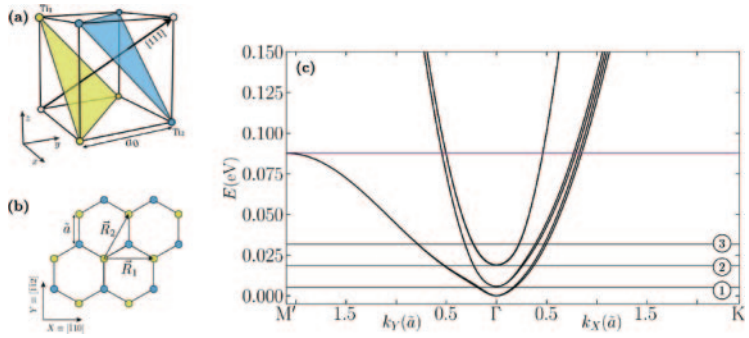

Fig. 3. – (a) Ti atoms in STO lattice, whose lattice constant is $a_0 = 0.3905\,\text{nm}$. (b) Projection of the two non-equivalent planes of Ti over the (111) plane with our choice of primitive vectors $\vec{R}_1$ and $\vec{R}_2$ and $\tilde{a} = \sqrt{2/3}a_0$. (c) Band structure along two different directions in the Brillouin zone. The purple benchmark line corresponds to a Lifshitz transition. The lines 1, 2 and 3 refer to benchmark chemical potential values in figs. 4 and 5. Figure adapted from [15].

structure is depicted in fig. 3(a) and (b). The Hamiltonian we took in consideration composes of the following terms:

$$H = H_{\text{TB}}(t_2, t_3) + H_{\text{SOC}}(\lambda) + H_{\text{TRI}}(\Delta) + H_v(v), \tag{3}$$

where H_{TB} contains the direct and indirect first neighbour hopping terms, whose amplitude $t_2 = 0.04\,\text{eV}$ and $t_3 = 0.5\,\text{eV}$. H_{SOC} is the atomic spin-orbit coupling of amplitude $\lambda = 0.01\,\text{eV}$ and H_{TRI} is the trigonal cristal field of amplitude $\Delta = -0.005\,\text{eV}$. Finally, H_v parametrizes the effect of the confinement which breaks the inversion symmetry and thus generates the so-called orbital Rashba [4], whose amplitude depends on the electric potential v. The expression of the full Hamiltonian can be find in ref. [15]. The last term is responsible for the EE. In the region of low filling, a quadratic expansion in the quasi-momentum $\vec{k}$ of the Hamiltonian leads to the effective Hamiltonian

$$H_{\text{eff}} = \sum_{i=x,y,z} \mathcal{E}_i(\vec{k})(\mathbb{1} - L_i^2) - \frac{\lambda}{2}\hat{L}\cdot\hat{S} - \frac{3\Delta}{2}L_{111}^2 + \mathcal{F}(\vec{k}\times\hat{L})\cdot\hat{n}_{111} + \varepsilon_0, \tag{4}$$

where $\vec{k}$ is expressed in units of the in-plane lattice constant $\tilde{a} = \sqrt{2/3}a_0 = \sqrt{2/3}\cdot 0.3905\,\text{nm}$, $\mathcal{E}_i$([1]) is the renormalized dispersion expanded to second order at $\vec{k}$, $\mathbb{1}$ is the identity matrix, L_i and S_i are the i-th components of the orbital and spin angular momentum operator for $L = 1$ and $S = 1/2$, L_{111} is the projection of the angular momentum along the (111) direction, $\hat{n}_{111}$ is a unitary vector along the (111) direction, the term $\vec{k}\times\hat{L}$ is the orbital Rashba whose strength is included in the coefficient $\mathcal{F} = 0.0035\,\text{eV}$ (depending on v which is fixed to $0.2\,\text{eV}$), and ε_0 is an energy constant. The electronic band structure in the low energy region is shown in fig. 3(c). By fixing the chemical potential to a benchmark value, we observe a non-trivial spin and orbital angular

([1]) $\mathcal{E}_x = 0.13k_X^2 - 0.29k_Xk_Y + 0.29k_Y^2$, $\mathcal{E}_y = 0.13k_X^2 + 0.29k_Xk_Y + 0.29k_Y^2$, $\mathcal{E}_z = 0.37k_X^2 + 0.044k_Y^2$.

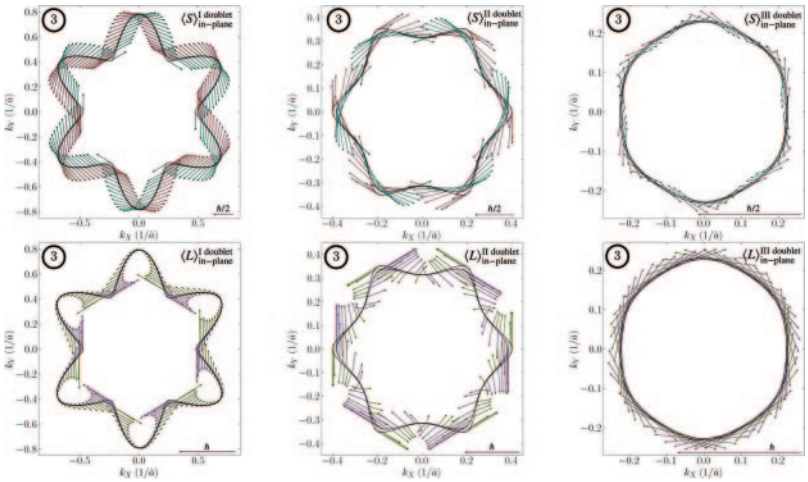

Fig. 4. – In-plane spin (upper panel) and orbital angular momentum (lower panel) textures for the three doublets with the chemical potential fixed to the value corresponding to the benchmark line 3 in fig. 3. The red and green arrows represent the mean value of in-plane component of the operator for the external band, while the blue and pink refer to the inner band. The mean value of the generic operator O is evaluated as $\langle O\rangle = \sqrt{\langle O_{\bar{1}10}\rangle^2 + \langle O_{\bar{1}\bar{1}2}\rangle^2}$. Figure adapted from [15].

momentum texture on the Fermi surface in fig. 4. Therefore, we can expect both spin and orbital EE for our system. The Edelstein susceptibility can be computed in the Boltzmann framework as for the model (1) leading to the susceptibility

$$\chi^{\mathcal{O}}_{\alpha\beta} = \left(-\frac{\tau_0 e \mu_b}{\tilde{a}\hbar^2} S_{cell} \sum_n \int_{BZ} \frac{\mathrm{d}^2\vec{k}}{(2\pi)^2} \frac{\partial f_{\mathrm{th}}}{\partial k_\beta} \langle \mathcal{O}_\alpha \rangle_n (\vec{k}) \right), \tag{5}$$

where $\mathcal{O}_\alpha = 2S_\alpha$ or L_α. The susceptibilities both for the spin and the orbital susceptibility as a function of the chemical potential μ are shown in fig. 5. We fixed $\tau_0 = 3.4 \times 10^{-12}$ s [16] and the temperature to $T = 10\,\mathrm{K}$. We decomposed $\chi_{\alpha\beta}$ into contributions of the three Kramers doublets in order to understand their non-monotonic behaviour. The spin susceptibility changes sign and presents a maximum and a minimum suggesting that, in real systems, a magnetization reversal can be induced through controlling the back gate voltage, *i.e.*, the chemical potential. On the other hand the orbital susceptibility is one order of magnitude greater than the spin susceptibility above the benchmark line 3 in the low energy region and above $\mu \sim 0.08\,\mathrm{eV}$.

4. – Discussion and conclusions

In this paper we introduced the Rashba EE and predicted a spin and orbital EE at (111) LAO/STO interface. We introduced a minimal model for the low-energy region able to predict non-trivial spin and orbital patterns responsible for a tunable spin EE and an even larger OEE, different from the canonical EE in a simple Rashba model. The main differences are the orbital character of the bands, responsible for the orbital magnetization, and the multiband model. In fact, the hybridization of the bands can be

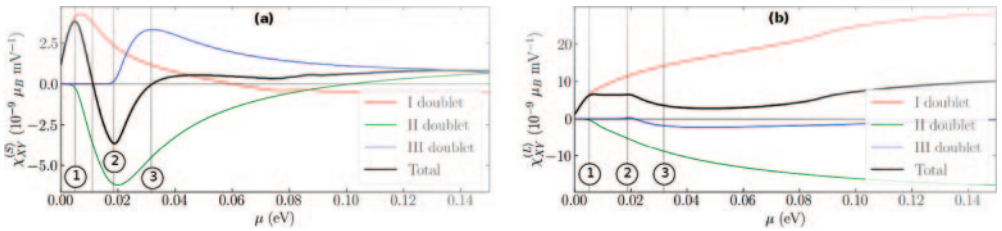

Fig. 5. – Spin (a) and orbital (b) Edelstein coefficient as a function of the chemical potential. The different colors correspond to the contribution of a specific Kramers doublet. Figure adapted from [15].

proved [15] as the mechanism responsible for the change in sign of the spin susceptibility, and in particular of the negative contribution of the green curve in fig. 5(a). By tuning to zero the spin EE only the OEE survives, providing a chance of disentangling the two components that are usually hard to distinguish [4]. Therefore, we showed that (111) LAO/STO interface can be suitable both for theoretical investigation of the orbital magnetization, and as a suitable platform for spintronics applications.

* * *

MT acknowledges Vittorio Cataudella, Carmine Antonio Perroni, Francesco Romeo and Roberta Citro as coauthors of the work which inspired this paper. MT acknowledges financial support from "Fondazione Angelo Della Riccia".

REFERENCES

[1] Baibich M. N., Broto J. M., Fert A., Van Dau F. N., Petroff F. *et al.*, *Phys. Rev. Lett.*, **61** (1988) 21.
[2] Hirohata A., Yamada K., Nakatani Y., Prejbeanu I., Diény B. *et al.*, *J. Magn. Magn. Mater.*, **509** (2020) 166711.
[3] Dieny B., Prejbeanu I. L., Garello K., Gambardella P., Freitas P. *et al.*, *Nat. Electron.*, **3** (2020) 8.
[4] Go D., Jo D., Lee H., Kläui M. and Mokrousov Y., *EPL*, **135** (2021) 37001.
[5] Edelstein V. M., *Solid State Commun.*, **73** (1990) 3.
[6] Vaz D. C., Barthélémy A. and Bibes M., *Jpn. J. Appl. Phys.*, **57** (2018) 9.
[7] Ohtomo A. and Hwang H. Y., *Nature*, **427** (2004) 6973.
[8] Nakagawa N., Hwang H. Y. and Muller D. A., *Nat. Mater.*, **5** (2006) 3.
[9] Walker S. M., De La Torre A., Bruno F. Y., Tamai A., Kim T. K. *et al.*, *Phys. Rev. Lett.*, **113** (2014) 17.
[10] Trama M., Cataudella V., Perroni C. A., Romeo F. and Citro R., *Nanomaterials*, **13** (2023) 5.
[11] Trama M., Cataudella V. and Perroni V. C. A., *Phys. Rev. Res.*, **3** (2021) 4.
[12] Lesne E., Sağlam Y. G., Battilomo R., Mercaldo M. T., van Thiel T. C., Filippozzi U. *et al.*, *Nat. Mater.*, **22** (2023) 5.
[13] Trama M., Cataudella V., Perroni C. A., Romeo F. and Citro R., *Phys. Rev. B*, **106** (2022) 7.
[14] Zhai J., Trama M., Liu H., Zhu Z., Zhu Y. *et al.*, *Nano Lett.*, **23** (2023) 24.
[15] Trama M., Cataudella V., Perroni C. A., Romeo F. and Citro R., *Nanomaterials*, **12** (2022) 14.
[16] Khan T., Zhang H., Zhang H., Yan X., Hong D. F. *et al.*, *Nanotechnology*, **28** (2017) 435701.